Ti/TiO2 nanotubes sensitized PbS quantum dots as photoelectrodes applied for decomposition of anticancer drugs under simulated solar energy

Paweł Mazierski [a], Patrycja Wilczewska [b], Wojciech Lisowski [d], Tomasz Klimczuk [e], Anna Białk-Bielińska [c], Adriana Zaleska-Medyska [a], Ewa M. Siedlecka [b], Aleksandra Pieczyńska [a,*]

[a] Department of Environmental Technology, Faculty of Chemistry, University of Gdansk, 80-308 Gdansk, Poland
[b] Department of General and Inorganic Chemistry, Faculty of Chemistry, University of Gdansk, 80-308 Gdansk, Poland
[c] Department of Environmental Analysis, Faculty of Chemistry, University of Gdansk, 80-308 Gdansk, Poland
[d] Institute of Physical Chemistry, Polish Academy of Science, Kasprzaka 44/52, 01-244 Warsaw, Poland
[e] Department of Solid State Physics, Gdansk University of Technology, 80-233 Gdansk, Poland

ABSTRACT

One of the challenges in research into photoelectrocatalytic (PEC) degradation of pollutants is finding the appropriate photoanode material, which has a significant impact on the process efficiency. Among all others, photoelectrodes based on an ordered TiO2 nanotube arrays are a promising material due to well-developed surface area and efficient charge separation. To increase the PEC activity of this material, the SILAR method was used to decorate Ti/TiO2 nanotubes by PbS quantum dots (QD). The ifosfamide (IF) degradation rate constants was twice as higher for PbS-Ti/TiO2 (0.0148 min^{-1}) than for Ti/TiO2 (0.0072 min^{-1}). Our research showed the highest efficiency of PEC degradation of drugs using IIIPbS-Ti/TiO2 made with 3 SILAR cycles (PbS QD size mainly 2–4 nm). The 4 and 6 of SILAR cycles resulted in the aggregation of PbS nanoparticles on the Ti/TiO2 surface and decreased IF PEC degradation rate to 0.0043 and 0.0033 min^{-1}, respectively. Research on PEC mechanism has shown that the drugs are degraded mainly by the activity of photogenerated holes and hydroxyl radicals. In addition, the identified drug intermediates made possible to propose a degradation pathways of anticancer drugs and the ecotoxicity test show no inhibition of *Lemna minor* growth of treated solutions.

1. Introduction

More and more attention in treatment industrial water and wastewater is paid to photochemical processes. They allow decomposition of persistent and toxic contaminants, resistant to degradation by conventional methods such as biological or physico-chemical, without the use of additional chemicals. In addition, the possibility of using solar radiation in these processes indicates that they are recognized as environmentally friendly technologies. One of these methods is photoelectrocatalysis (PEC), which combines electrochemical oxidation (EO) and heterogeneous photocatalysis (PC) (Garcia-Segura and Brillas, 2017). High efficiency in the photoelectrocatalytic degradation of organic pollutants is the result of synergistic effect between photocatalytic and electrochemical processes. This is due to the reduction of the recombination of photo-generated electrons-holes pairs on the photocatalyst used as a photoanode, by the application of an external

bias potential (Liu et al., 2018). It is worth noting that in the case of PEC, much lower potentials are used than in electrochemical oxidation which equates to less energy consumption. Limiting recombination process increases the life time of photo-generated electrons and holes, which in turn provides the greater its activity. The higher photoelectrocatalytic degradation efficiency than photocatalytic was confirmed by many studies (Mazierski et al., 2019; Daghrir et al., 2014; Wu et al., 2016; Cheng et al., 2013; Su et al., 2016; Xin et al., 2011). Photoelectrocatalytic degradation has been used to decomposed dyes (Liu et al., 2017; Ma et al., 2017), pesticides (Ye et al., 2018), pharmaceuticals (Su et al., 2016; Olvera-Rodríguez et al., 2019), chemicals (Mohite et al., 2015) and even real wastewater (Garcia-Segura and Brillas, 2017; Daghrir et al., 2014; Collivignarelli et al., 2021) and landfill leachate (Zhou et al., 2015). Among pharmaceuticals, tetracyclines, sulfamethoxazole, diclofenac and paracetamol were removed by PEC (Garcia-Segura and Brillas, 2017). According to our best knowledge there is no

information on the PEC degradation of anticancer drugs except our previous work (Mazierski et al., 2019). Anticancer drugs are a group of new micro-pollutants resistant to conventional technologies used in treatment plants. Therefore, more and more of these compounds are detected in the aquatic environment (Pieczyńska et al., 2017). Their main source in surface waters are ineffective treated hospital, domestic and industrial wastewaters. Thus, the development of effective method for their removal, would limited their presence in the environment. The risk associated with the presence of anticancer drugs in the environment is due to their fetotoxic, genotoxic and teratogenic properties, which is hazardous for all living organisms including people (Santos et al., 2017). Three anticancer drugs, 5-fluorouracil (5-FU), ifosfamide (IF) and imatinib (IMB), with different chemical structures and physico-chemical properties, were selected for the study. All of the selected drugs were detected in environmental samples (surface water, wastewaters) at the level of µg/ng per liter, but their concentration is predicted to increase due to the growing incidence of cancer and increasing consumption of these drugs (Isidori et al., 2016).

The efficiency of the PEC degradation process depends on various parameters (Daghrir et al., 2012) and one of the most important is photoanode material (Zhang et al., 2012). The properties of the photocatalyst used as a photoanode strongly influence on both the efficiency and mechanism of PEC. As with heterogeneous photocatalysis, pristine or modified TiO_2 are the most commonly used in photoelectrocatalysis as photoanode (Garcia-Segura and Brillas, 2017), due to the high stability, low cost, no toxicity and good photocatalytic properties. Thus far, different TiO_2 structures have been applied as photoanodes materials, such as porous thin film (Chatzitakis et al., 2017), nanorods (Deng et al., 2018b), nanosheets and nanotubes (Mazierski et al., 2019). Highly ordered nanotubes of TiO_2 obtained by anodization of Ti film exhibited high photocatalytic activity and stability, therefore is promising materials to PEC application. Nevertheless, TiO_2 activity mainly under the UV radiation limits using the solar radiation in such a system. One of the strategy of enhancing the activity of TiO_2 nanotubes in the visible light range is the formation of nanocomposites with narrow band gap semiconductors such as metal oxides CeO_2 (Deng et al., 2018a), WO_3 (Martins et al., 2017), Cu_2O (Ma et al., 2018), Co_3O_4 (Huang et al., 2015), MnO_2 (Ma et al., 2017) and sulfides CdS (Yu et al., 2015), PbS (Zhang et al., 2019a), SnS (Zhang et al., 2019b), Bi_2S_3 (Mazierski et al., 2017). Among narrow band semiconductors, lead sulfide is a promising material to sensitize TiO_2 nanotubes due to properties such as long exciton lifetime (200–800 ns), band dgap in the 0.3–2.0 eV range depending on the quantum dots (QD) size and matching energy band with TiO_2 (Liu et al., 2016). Moreover, it was found that heterojunction between PbS and TiO_2 nanoparticles can significantly enhanced the exciton absorption range and induce the electron transport reducing recombination of photogenerated charges (Liu et al., 2016). Enhanced photocatalytic activity of $PbS-TiO_2$ nanocomposites compared to TiO_2 was already presented (Xu et al., 2014; Hajjaji et al., 2020). Zhang et al. (2019a) shown higher photocatalytic degradation efficiency of 4-chlorobenzoic acid using TiO_2 nanotubes decorated by PbS nanoparticles than pure TiO_2. So far, TiO_2 NTs sensitized by PbS were applied in photocatalytic degradation (Zhang et al., 2019a; Rahna et al., 2016) and as electrodes in solar cells (Rahna et al., 2016; Zhou et al., 2016a). To the best of our knowledge, such nanocomposites has not been applied for photoelectrocatalytic degradation of organic pollutants. Moreover, there has not been no study about photoelectrocatalytic mechanism and correlation of surface and electrochemical properties with photoelectrochemical activity of PbS/TiO_2 nanocomposites.

Depositing narrow band gap semiconductors in the form of quantum dots (QDs) on a TiO_2 matrix gives the opportunity to obtained materials with unique properties. Changing size and distribution of QDs on matrix the properties such as light absorption, band gap and band edges of QD are modified (Zhang et al., 2016). The most common method used for sensitized TiO_2 NTs by QD is the successive ionic layer adsorption and reaction method (SILAR). Parameters of this process such as number of

SILAR cycles, dipping time, type and concentration of precursor, allows to control the distribution and size of deposited QDs (Xu et al., 2014; Rahna et al., 2016). Furthermore, SILAR method gives possibility to deposit nanostructures with high loading and low aggregation and is inexpensive. Rahna et al. (2016) reported that photocatalytic activity and stability of TiO_2 sensitized by PbS depends on number of SILAR cycles. Zhang et al. (2016) showed influence of precursors Pb and S concentration ratio in SILAR method on size and distribution of PbS QD and photoelectrochemical properties. However, no correlation between PbS nanoparticle size and photoactivity was determined.

In view of this, we have prepared a series of photoelectrodes based on titanium dioxide nanotubes sensitized by PbS QDs with increased visible light activity and applied for photoelectrocatalytic degradation of selected anticancer drugs. Anodization was used for the preparation of TiO_2 nanotubes followed by PbS quantum dots deposition via SILAR method. The amount, size and distribution of PbS QD deposited on the TiO_2 matrix was controlled by the number of SILAR cycles which had an impact on the properties and activity of photoelectrodes. Techniques such as scanning electron microscopy (SEM), transmission electron microscopy (TEM), X-ray diffraction patterns (XRD), X-ray photoelectron spectroscopy (XPS), UV-Vis absorbance and photoelectrochemical analyses were used to characterize structure and morphology of the prepared materials. Except, the effect of electrode material and type of degraded drug, the effect of potential and pH solution on photoelectrocatalysis efficiency was studied. In addition, the mechanism of photoelectrocatalytic degradation of drugs and their degradation pathway were examined, and variations in eco-toxicity against *Lemna minor* during the process were determined.

2. Materials and methods

2.1. Chemicals and materials

The standards of anticancer drugs 5-FU (99%), IF (99%) and IMB (98%) were purchased from Sigma Aldrich (Steinheim, Germany). Analytical grade methanol, sodium sulfate, ascorbic acid, formic acid (80%) and HPLC grade acetonitrile were obtained from POCH S.A. (Gliwice, Poland). Titanium foils (0.127 mm thickness, 99.7% purity,) were purchased from Sigma-Aldrich. Isopropanol, acetone, methanol, were purchased from P.P.H. STANLAB, ethylene glycol (EG), $Pb(NO_3)_2$, $Na_2S \cdot 9H_2O$ from CHEMPUR, and ammonium fluoride were analytical grade and purchased from Across Organics.

2.2. Preparation of PbS-Ti/TiO₂ photoelectrodes

$PbS-Ti/TiO_2$ photoelectrodes were prepared via the electrochemical anodization of titanium foil followed by PbS QDs deposition by a SILAR technique. Titanium foils (2 × 5 cm) were cleaned in acetone, isopropanol, methanol and deionized water, for 10 min before use and then dried in an air stream. Anodic oxidation was performed in a three-electrode electrochemical set-up, where Ti foil was used as the working electrode, Pt mesh as the counter electrode and Ag/AgCl as the reference electrode. An electrolyte was composed of EG, NH_4F (0.09 M) and H_2O (2 vol%). The process was mentioned at 30 V using a programmable power supply (MCP M10-QS1005). The obtained samples were flushed by deionized water, sonicated in water for 5 min, dried in air (80 °C, 24 h) and calcined at 450 °C for 1 h.

The TiO_2 NT were immersed in a methanol solution containing lead nitrate (0.02 M) for 1 min, and then the samples were rinsed with pure methanol and dried. Second, the samples were immersed into a 0.02 M $Na_2S \cdot 9H_2O$ methanol solution for 1 min, rinsed with methanol, and dried. This procedure was repeated 2,3,4 and 6 no. of times, and finally, the samples were dried at 80 °C.

2.3. Characterization of the PbS-Ti/TiO₂ photoelectrodes

The field emission scanning electron microscope (SEM, JSM-7610F, JEOL) were used to determined morphology of the obtained PbS-Ti/TiO₂ photoelectrodes and the high-resolution transmission electron microscopy (TEM, Hitachi H-800) were applied to defined size and distribution of PbS QDs in the PbS-Ti/TiO₂ nanocomposites.

The UV-Vis absorbance spectra of the PbS-Ti/TiO₂ photoelectrodes were recorded at room temperature in a range of 300–800 nm, with a scanning speed of 250 nm min^{-1}, on a UV-Vis spectrophotometer (Shimadzu UV 2600).

X-ray diffraction (XRD) analysis was performed at room temperature using a Bruker D2 Phaser diffractometer equipped with Cu K$_{\alpha}$ radiation source and a LynxEye-XE detector. The data were collected in a range 5 < 2Θ < 70 degrees with the scan speed 3 deg./min and a scan step 2Θ = 0.01 deg. The XRD patterns were analyzed by the LeBail method using the HighScore package.

The XPS spectrometer (PHI 5000 VersaProbe, ULVAC-PHI, Chigasaki Japan) was used to confirm the formation of PbS compound and for examining the surface states of elements present on the surface of PbS-Ti/TiO₂ photoelectrodes. The high-resolution (HR) XPS spectra were recorded using monochromatic Al-Kα radiation (hν = 1486.6 eV) with the hemispherical analyzer at the pass energy of 23.5 eV and the energy step size of 0.1 eV. Binding energy (BE) scale was referenced to the C 1s peak with BE = 284.8 eV.

The photoelectrochemical properties of the PbS-Ti/TiO₂ photoelectrodes were investigated using an AutoLab PGSTAT 204 potentiostat-galvanostat (Methrom Autolab) in a three-electrode system where PbS-Ti/TiO₂ photoelectrodes were used as the working electrode, Ag/AgCl/3.0 M KCl and Pt mesh were used as the reference and counter electrodes, respectively. Before use, the electrolyte composed of 0.5 M Na₂SO₄ aqueous solution was purged with argon for 1 h. The photoactivity measurements were performed using a 150 W Xenon lamp (Hamamatsu Photonics K.K., model E7536) equipped with a water IR cut-off filter. The irradiation intensity was measured by an optical power meter (Hamamatsu, C9536-01) and adjusted to 100 mW cm^{-2}.

2.4. Determination of ·OH and O₂·⁻

The determination of hydroxyl radicals (·OH) generated in PEC using PbS-Ti/TiO₂ photoelectrodes were performed by a fluorescence technique with terephthalic acid according to Mazierski et al. (2019). For the experiment photoelectrocatalytic setup were used with 80 mL aqueous solution of 50 mM terephthalic acid and 42 mM Na₂SO₄.

Superoxide radicals (O₂·⁻) generated in PC and PEC with PbS-Ti/TiO₂ photoelectrodes were measured by spectrophotometric technique with nitroblue tetrazolium chloride (NBT, 0.025 mM) (Jia et al., 2015). NBT, with an absorption maximum at 259 nm, reacts selectively with superoxide radicals resulting decreasing of NBT concentration analyzed by detecting the absorption. Decreasing NBT concentration is proportional to the amount of produced superoxide radicals. Measurements were performed in PEC reactor with three electrode system with 80 mL of aqueous solution of NBT (0.025 mM) and Na₂SO₄ (42 mM) worked with + 1 V /Ag = AgCl at 550 W m^{-2} light intensity.

2.5. Photoelectrocatalytic activity

The photocatalytic degradation of anticancer drugs (5-FU, IF and IMB) were performed in thermostatic single-compartment reactor with magnetic stirring. For each process 80 mL of drug solution at 20 mg L^{-1} prepared in supporting electrolyte (Na₂SO₄, 42 mM) were used. To investigate the effect of pH, to IF solution (pH 6.0) sulfuric acid or sodium hydroxide were added to obtained pH 3 and 9. The reactor contained system of three electrodes where one of PbS-Ti/TiO₂ photoelectrodes, stainless steel (SS) and silver chlorine electrode (Ag/AgCl, 0.3 M KCl) were applied as anode, cathode and references

electrode, respectively and power supply (Ami TTi PL303, Huntington, England) provide constant potential in range from + 0.5 to + 1.5 V /Ag|AgCl. A Suntest CPS+ solar simulator (Atlas Material Testing Technology LLC) equipped with a xenon lamp with light intensity 550 W m^{-2} as the UV-Vis irradiation source was used. Additionally, in the same reactor photocatalytic (without applied potential) and electrochemical (without irradiation) degradation of anticancer drug were investigated.

The contribution of individual oxidants generated in photoelectrocatalysis were examined by conducting a PEC degradation of each anticancer drugs with scavengers. The methanol (10 mM), ascorbic acid (1 mM), formic acid (10 mM) and mixtures of methanol (10 mM) and formic acid (10 mM) were used as scavengers respectively ·OH, O₂·⁻, h⁺ and both ·OH and h⁺.

2.6. Analytical methods and eco-toxicity

The concentration of 5-FU, IF and IMB during the processes was determined by HPLC-UV analysis (Shimadzu) equipped with a Kinetex XB-C-18 column (150 × 3 mm, 5 μm) (Phenomenex). In the case of 5-FU as a mobile phase acetonitrile and water in ratio 6:94 in isocratic program was used, with the flow rate 0.2 mL min^{-1} and injection volume 25 μL. In analytical method of IF, the same mobile phase as for 5-FU were used in ratio 20:80 acetonitrile to water. The flow rate was 0.5 mL min^{-1} and injection volume 50 μL. The IMB was analyzed using 1% acetic acid water solution and acetonitrile (85:15) with flow rate 0.9 mL min^{-1} and 30 μL of injection of sample. The detection system was operated at 266 nm for 5-FU, 200 nm for IF and 265 nm for IMB. The detection limit of the HPLC-UV methods for 5-FU, IF and IMB were 0.017, 0.17 and 0.83 mg L^{-1}, respectively.

The organic degradation products of drugs were identified based on liquid chromatography coupled to mass spectrometer (LC-MS) analysis (Agilent 1200 Series LC system, Agilent Technologies, Inc., Santa Clara, USA, HCT Ultra ion trap MS, Brucker Daltonics, Bremen, Germany). The LC and MS parameters were according to method used by Siedlecka et al. (2018).

Total organic carbon (TOC) were determined by TOC analyzer equipped with an autosampler (Shimadzu, Germany) and (ΔTOC)$_{exp}$ (mg L^{-1}) was the experimental difference between TOC before and after PEC process. The TOC data were used for mineralization current efficiency (MCE) calculation applying the equation (Eq. (1)) (Siedlecka et al., 2018):

$$MCE \quad [\%] = \frac{n \quad F \quad V_s}{4.32 \quad 10^7} \frac{(\Delta TOC)_{exp}}{m \quad I \quad t} \quad 100 \tag{1}$$

where n was the number of electrons consumed per one molecule of drug assuming the total mineralization (n$_{5-FU}$ = 8, n$_{IF}$ = 36, n$_{IMB}$ = 124), F was the Faraday constant (96,487 C mol^{-1}), 4.32 × 10⁷ was a factor to homogenize units (3600 s h^{-1} x 12,000 mg mol^{-1}), m was the number of carbon atoms of 5-FU (m$_{5-FU}$ = 4), IF (m$_{IF}$ = 7) and IMB (m$_{IMB}$ = 29), V$_s$ (dm³) was the treated solution volume, I (A) was current and t (h) time of PEC process.

The amount of electrical energy (E$_{EO}$, kWh m^{-3} order^{-1}) consumed for PEC and PC degradation of drugs were estimate based on the power of the lamp used for irradiation (P$_{Lamp}$ (kW)) and the power electrochemical cell (P$_{Cell}$ (kW)), according to Eq. (2) (Mazierski et al., 2019):

$$E_{EO} = \frac{(P_{Lamp} + P_{Cell}) \quad t}{V_s \quad \log\left(\frac{C_0}{C_t}\right)} \tag{2}$$

where C₀ and C$_t$ are initial and after treatment concentrations of drugs respectively, V$_s$ (m³) was the volume of treated solution in time (t (h)).

The eco-toxicity of 5-FU, IF and IMB initial and treated by photoelectrocatalysis solutions towards duckweed *Lemna minor* was investigated according to our previously reported procedure (Mazierski et al.,

2019).

3. Results

To increase photoelectrocatalytic activity of Ti/TiO$_2$, PbS QDs were deposited using the SILAR method. Due to the fact, that the number of SILAR cycles is the main parameter determining the size and amount of deposited nanoparticles, photoelectrodes IIPbS-Ti/TiO$_2$, IIIPbS-Ti/TiO$_2$, IVPbS-Ti/TiO$_2$ and VIPbS-Ti/TiO$_2$ were prepared using 2, 3, 4 and 6 cycles, respectively. The obtained photoelectrodes were varies in size and amount of PbS nanoparticles, and thus in photoelectrocatalytic activity.

3.1. Characteristics of PbS-Ti/TiO$_2$ photoelectrodes

3.1.1. Scanning electron microscopy (SEM) and transmission electron microscopy (TEM)

The geometrical parameters of TiO$_2$ nanotubes was determined on the basis of SEM images (Fig. 1), which was consistent with our previous results (Mazierski et al., 2019) where average length, wall thickness and diameter of nanotubes was 1.7 μm, 65 nm and 7.5 nm, respectively. The nanotube size was the same for all PbS-Ti/TiO$_2$ and pristine Ti/TiO$_2$ photoelectrodes, and the estimated developed surface area was 549 cm^2. The SEM images exhibited that the nanotubes were vertically oriented and top-end-open. In addition, in the case of the IVPbS-Ti/TiO$_2$ electrode prepared using 4 SILAR cycles, the formation of larger agglomerates of PbS nanoparticles on top of TiO$_2$ nanotubes was observed. With the increase in the number of SILAR cycles this phenomenon intensified and in the case of the VIPbS-Ti/TiO$_2$ photoelectrode, number of agglomerates of PbS nanoparticles covering nanotube surfaces increase.

Fig. 2 shows TEM images and size distribution of PbS nanoparticles on the TiO$_2$ nanotubes surface. The sizes of PbS nanoparticle ranged from < 2 to 12 nm, which classifies them as QDs. PbS QD were regularly distributed over the whole surface of TiO$_2$ nanotubes, and their size depended on the number of SILAR cycles. In the case of the IIPbS-Ti/TiO$_2$ photoelectrode, mostly QDs with the size in the range of <2–4 nm were observed. Increasing the number of SILAR cycles to 3 resulted in the formation of QDs with size from < 2 to 8 nm, but among then the largest fraction were QDs ranging in size from 2 to 4 nm. Photoelectrodes IVPbS-Ti/TiO$_2$ and VIPbS-Ti/TiO$_2$ were characterized by a similar size distribution of PbS QDs (Fig. 2). What is more, the formation of agglomerates on the TiO$_2$ nanotubes surface was observed for both

photoelectrodes, which could limit the growth of nanoparticles inside the nanotubes. Therefore, the increase of PbS QDs size was not observed when the number of SILAR cycles was increase from 4 to 6.

3.1.2. X-ray diffraction patterns (XRD)

Fig. 3 presents XRD patterns for all obtained samples (IIPbS-Ti/TiO$_2$, IIIPbS-Ti/TiO$_2$, IVPbS-Ti/TiO$_2$ and VIPbS-Ti/TiO$_2$). The XRD data are represented by open circles, and a profile fitting (Le Bail method) is shown by a blue line. For the analysis two models were used: TiO$_2$ – anatase (I41/amd) and Ti metal (P63/mmmc). The observed impurity phases are Pb$_3$O$_5$ and possibly PbSO$_3$ lead sulfate (IV) marked by * and ^ respectively. The strongest XRD reflections for PbS are expected for 2 Θ = 26 and 30 deg. As can be seen in a right panel of Fig. 3, small anomalies marked by arrows are likely due to presence of PbS. The anomalies are broad which is caused by small size of PbS QDs.

3.1.3. X-ray photoelectron spectra (XPS)

Fig. S1 shows Ti2p, O1s, Pb4f, S2p and Pb5d XPS spectra recorded on pristine Ti/TiO$_2$ NTs and on PbS-Ti/TiO$_2$ nanocomposites prepared using 2, 3, 4 and 6 SILAR cycles. The Ti 2p (a) and O 1s (b) spectra identify well the TiO$_2$ NTs (Naumkin et al., 2012), whereas the Pb4f (c), S 2p (d) and Pb 5d (e) spectra confirm the final deposition of PbS nanoparticles on the TiO$_2$ NTs. Elemental composition (in atomic %) in the surface layer of all samples investigated is presented in Table S1. One can see that the amount of Pb and S, originated from PbS deposited on Ti/TiO$_2$, increased with the increasing number of SILAR cycles. Examination of Pb4f and S2p HR spectra reveal the chemical character of Pb and S surface species after increasing the number of SILAR cycles (Fig. 4). Two states of Pb were identified in PbS-Ti/TiO$_2$ nanocomposites through Pb4f spectra deconvolution, Pb $4f_{7/2}$ peaks at 137.1–137.6 and 138.7–138.8 eV, which are assigned to PbS/PbOx and PbSO$_x$ species, respectively (Hajjaji et al., 2020; Naumkin et al., 2012; Reiche et al., 1999). Also the S 2p spectra exhibits two states represented by S $2p_{3/2}$ signals located at 160.8–161.2 eV and 168.1–168.6 eV, which are characteristic for PbS and PbSO$_4$ species, respectively (Hajjaji et al., 2020; Naumkin et al., 2012; Reiche et al., 1999; Zhou et al., 2016b). Inspection of XPS data presented in Table S2 clearly show that the PbSO$_x$ species are a dominant fraction of Pb and S components on the surface of IIPbS-Ti/TiO$_2$, IIIPbS-Ti/TiO$_2$ and IVPbS-Ti/TiO$_2$ samples whereas the PbS and PbO species are the main compounds on the surface of VIPbS-Ti/TiO$_2$ nanocomposites. Both pristine Ti/TiO$_2$ NTs and PbS-Ti/TiO$_2$ samples seems to be partially oxidized in view of the exposure to the
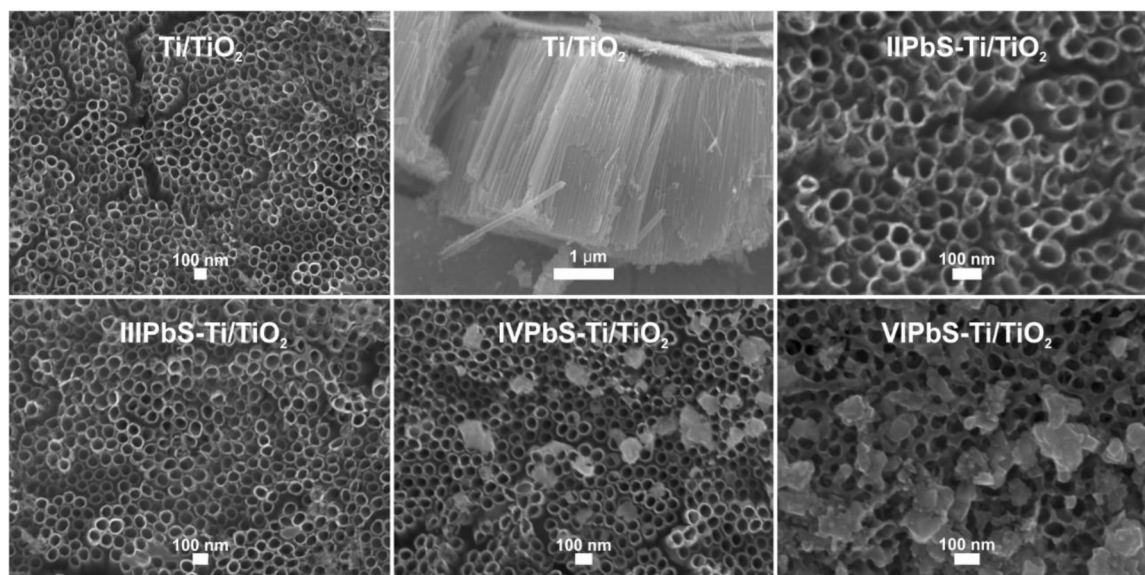

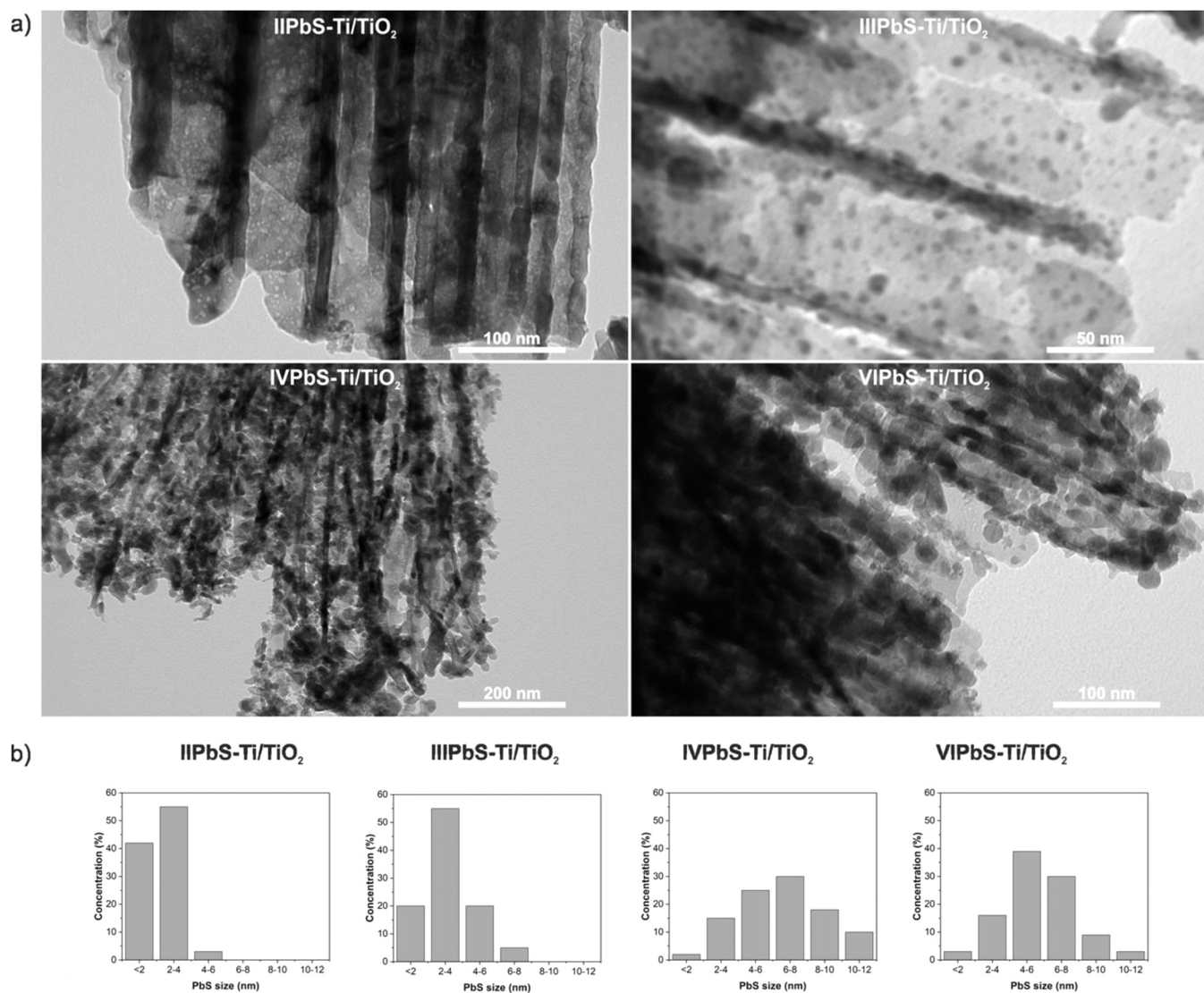**Fig. 1.** SEM images of photoelectrodes Ti/TiO$_2$ and PbS-Ti/TiO$_2$.

Fig. 2. TEM images (a) and PbS QDs size distribution (b) of photoelectrodes PbS-Ti/TiO$_2$.

ambient atmospheric conditions (see O/Ti > 2 ratio for pristine Ti/TiO$_2$ in Table S1). However, assuming this effect is comparable for all samples, we can observe the relative increase of oxygen species on PbS-Ti/TiO$_2$ samples processed using higher number of SILAR cycles (compare the O/Ti ratios in Table S1).

3.1.4. UV-Vis absorbance

The optical properties of PbS-Ti/TiO$_2$ and pristine Ti/TiO$_2$ photoelectrodes were estimate based on UV-Vis absorbance measurement. As show in Fig. S2, all samples have a characteristic energy band structures of TiO$_2$ in UV absorption region lower than 400 nm and the second region in the visible-light associated with trapped electrons at the Ti^{3+} center (Mazierski et al., 2019). Moreover, in the case PbS-Ti/TiO$_2$ nanocomposites, a significant red shift absorption in the visible light was observed what is associated with presence of PbS QDs on TiO$_2$ (Rahna et al., 2016). Additionally, increase of absorbance in the visible region (400–800 nm) with increase number of SILAR cycle (from 2 to 6) was caused by increased amount of PbS nanoparticle on TiO$_2$.

3.1.5. Photoelectrochemical analyses

The photocurrent response generated by the PEC process at +1 V on the Ti/TiO$_2$ and PbS-Ti/TiO$_2$ electrodes was shown in Fig. 5. All prepared electrodes showed good photo-response properties. Moreover, it

was observed that PbS-sensitized electrodes generated higher photocurrent than pristine Ti/TiO$_2$. This indicates a greater number of photogenerated electrons and their better separation from holes. The highest value of photocurrent (j = 1.25 mA cm^{-2}) was achieved for IIIPbS-Ti/TiO$_2$, then IIPbS- Ti/TiO$_2$ (j = 1.1 mA cm^{-2}), IVPbS- Ti/TiO$_2$ (j = 0.95 mA cm^{-2}), VIPbS – Ti/TiO$_2$ (j = 0.6 mA cm^{-2}) and Ti/TiO$_2$ (j = 0.4 mA cm^{-2}). These results indicated that a large amount of PbS ODs on the surface may disturb the flow of electrons as was in the case with IVPbS-Ti/TiO$_2$ and VIPbS-Ti/TiO$_2$. Such observations were also presented by Guo et al. (2021).

3.1.6. Hydroxyl and superoxide radicals measurements

Hydroxyl radicals, h$^+$ and superoxide radicals are major oxidants generated in PEC process (Garcia-Segura and Brillas, 2017). Hydroxyl radicals are mainly generated by the oxidation of water or hydroxyl ions by photogenerated holes (h$^+$) on the semiconductor surface and as a result of transformation of superoxide radicals which are generated by the reduction of oxygen molecules by the e$^-$ on the surface of semiconductor or cathode. As shown in Fig. 6a the amount of generated hydroxyl radicals were depended on the photoanode material and the greatest amount in the PEC process were generated on the IIIPbS-Ti/TiO$_2$ photoelectrode. In the case of other PbS-Ti/TiO$_2$ photoelectrodes, the amount of hydroxyl radicals was slightly higher than that
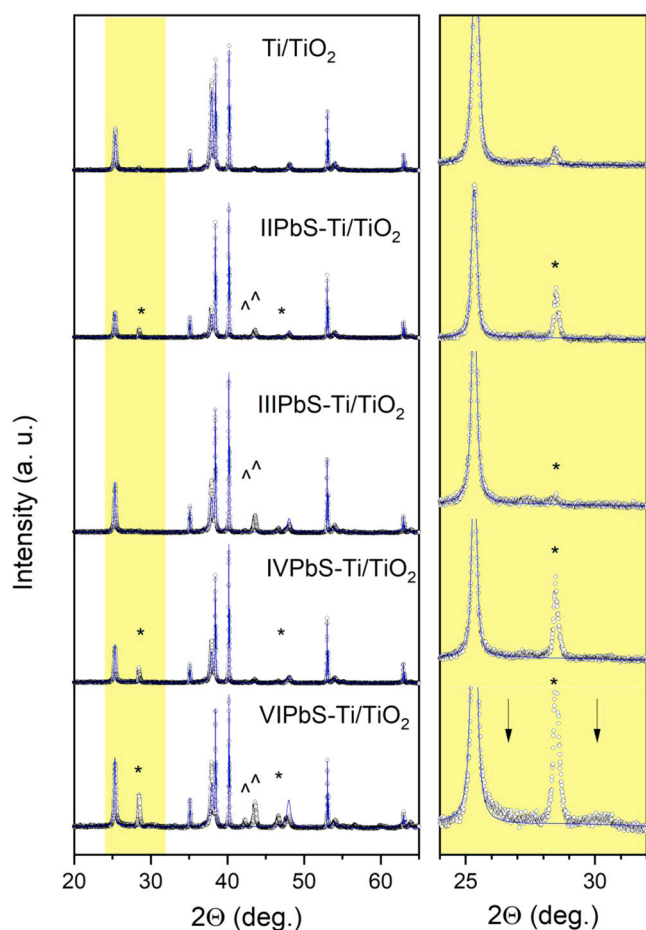
Fig. 3. X-ray diffraction patterns for Ti/TiO$_2$, IIPbS-Ti/TiO$_2$, IIIPbS-Ti/TiO$_2$, IVPbS-Ti/TiO$_2$ and VIPbS-Ti/TiO$_2$ sample. A blue line represents a Le Bail profile fitting. A right panel presents xrd data between 24 deg. < 2Θ < 32 deg. in the vicinity of expected PbS reflections (marked by arrows).

Fig. 4. High resolution Pb4f and S2p XPS spectra recorded on PbS-Ti/TiO$_2$ nanocomposites prepared using 2, 3, 4 and 6 SILAR cycles.

Fig. 5. Photocurrent response at + 1 V/Ag=AgCl of Ti/TiO$_2$ and PbS-Ti/TiO$_2$ photoelectrodes.

generated on pristine TiO$_2$.

In contrast to hydroxyl radicals, superoxide radicals were generated in a larger amount on the Ti/TiO$_2$ photoelectrode than on the PbS-Ti/TiO$_2$ (Fig. 6b). In the case of PbS-Ti/TiO$_2$ photoelectrodes, most of the superoxide radicals were generated in the presence of IIIPbS-Ti/TiO$_2$, slightly less for II-PbS-Ti/TiO$_2$. In contrast, the smallest amounts of O$_2^-$ were generated in the PEC process for IVPbS-Ti/TiO$_2$ and VIPbS-Ti/TiO$_2$ photoelectrodes, with the large amount of PbS nanoparticles on the TiO$_2$ surface. As presented by Xu et al. (2014) the thicker film of the PbS, the longer time for transporting electrons to TiO$_2$ and then to the cathode. As a result, PbS is becoming a barrier to charges transport. What's more, the amount of superoxide radicals generated in the photocatalytic and photoelectrocatalytic processes was compared using the IIIPbS-Ti/TiO$_2$ photoelectrode. As can be seen in Fig. 6c, definitely more radicals are generated in the PEC process, which indicates a reduction in the recombination of photogenerated charges and production of O$_2^-$ at the cathode.

3.2. Photoelectrochemical activity of PbS-Ti/TiO$_2$

Photoelectrocatalytic efficiency of prepared nanocomposites was tested in the process of IF degradation at a concentration of 20 mg L^{-1} at a potential of + 1 V /Ag=AgCl and simulating sunlight at an intensity of 550 W m^{-2}. As shown in Fig. 7a, the fastest degradation of IF occurred with the IIIPbS-Ti/TiO$_2$ photoelectrode, slightly slower with the IIPbS-Ti/TiO$_2$. Also the highest degree of TOC reduction and thus the highest mineralization current efficiency (MCE) was determined for the IIIPbS-
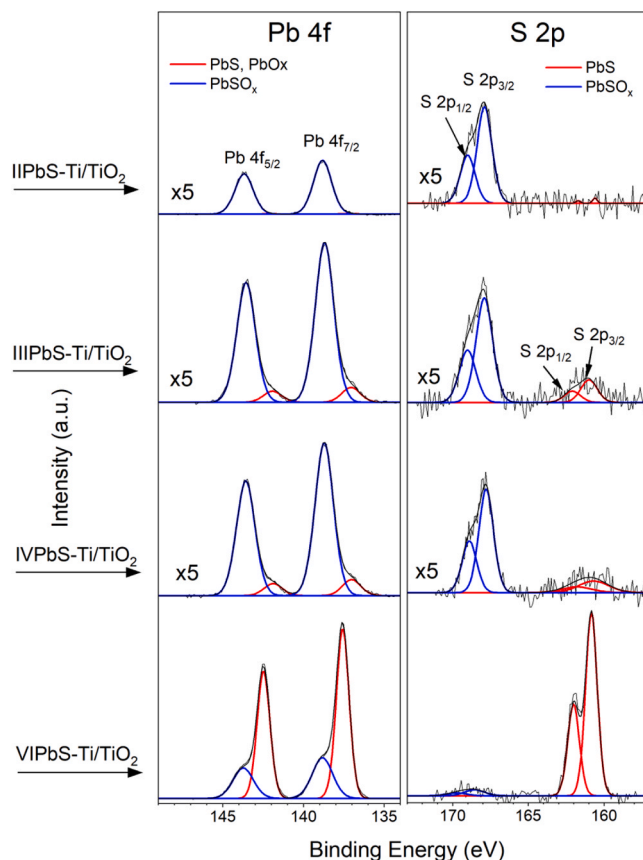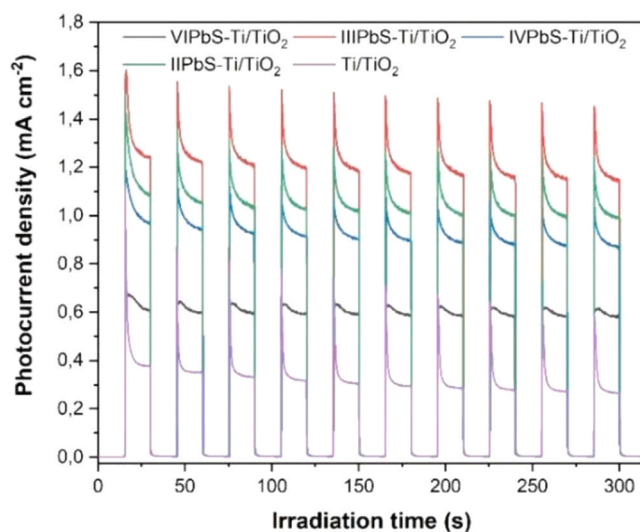
Ti/TiO$_2$ photoelectrode (Table S3). Both photoelectrodes, IIPbS-Ti/TiO$_2$ and IIIPbS-Ti/TiO$_2$ showed greater PEC activity than pristine Ti/TiO$_2$. The increase in the PEC activity of these electrodes resulted from the presence of PbS QDs whose sizes ranged from < 2 to 8 nm. However, for IIPbS-Ti/TiO$_2$ photoelectrode, QDs were in the vast majority from < 2 to 4 nm. On the other hand, when three SILAR cycles (IIIPbS-Ti/TiO$_2$) were used, the QDs were mainly from 2 to 4 nm while QDs from 4 to 8 nm appeared. This photoelectrode also generated the largest amount of
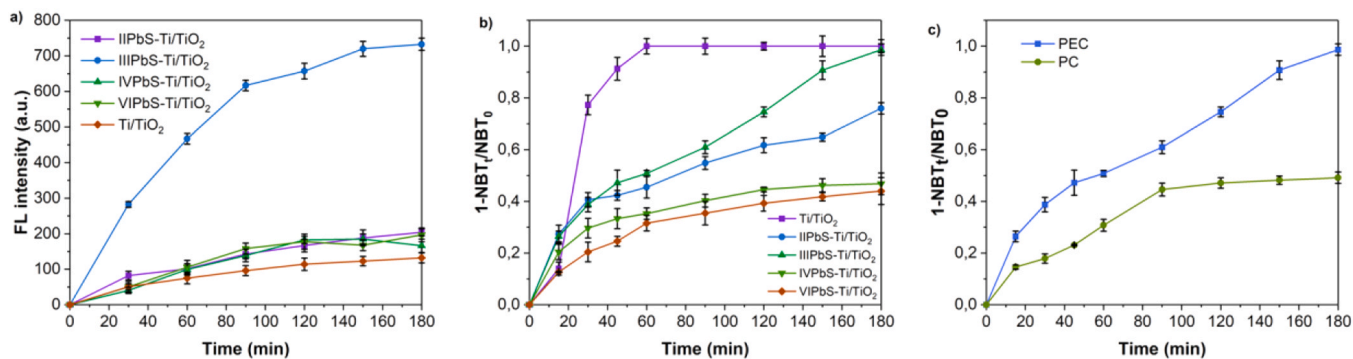
Fig. 6. Hydroxyl radicals (a) and superoxide radicals (b) generated in PEC at + 1 V/Ag|AgCl, 550 W m^{-2} using Ti/TiO$_2$ and PbS-Ti/TiO$_2$ photoelectrodes and superoxide radicals generated in PC at 550 W m^{-2} and PEC at + 1 V/Ag|AgCl, 550 W m^{-2} (c) using IIIPbS-Ti/TiO$_2$ photoelectrode.
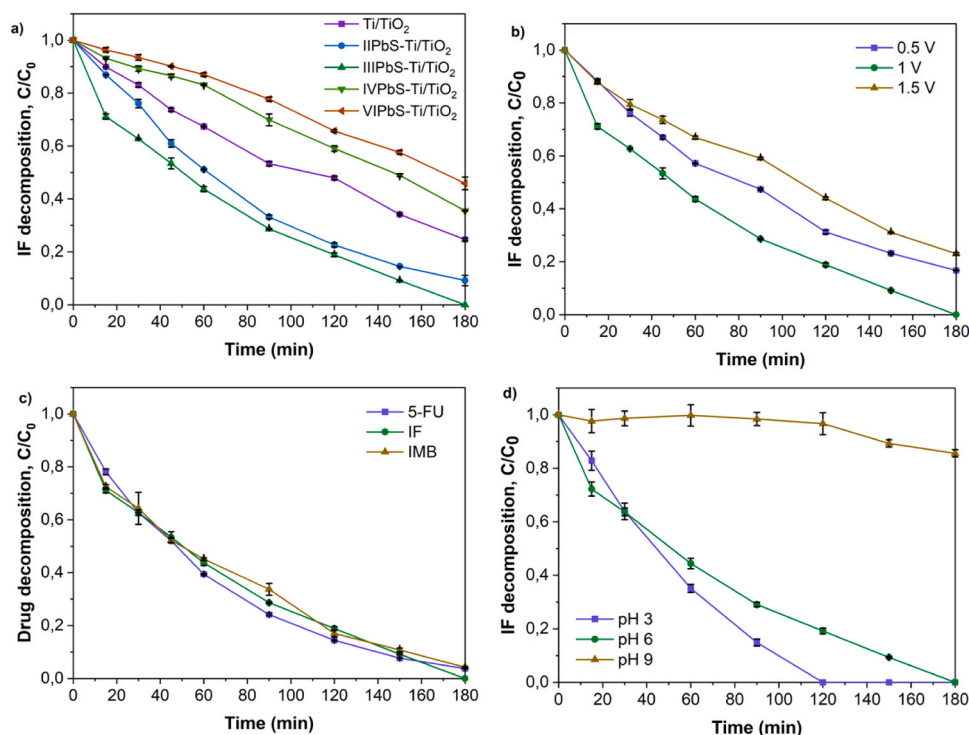

Fig. 7. Efficiency of drugs (20 mg L^{-1}) photoelectrocatalytic removal: the effect of PbS-Ti/TiO$_2$ photoelectrodes applied in PEC at + 1 V/Ag|AgCl and 550 W m^{-2} (a); applied potential using IIIPbS-Ti/TiO$_2$ at 550 W m^{-2} (b); type of anticancer drugs using IIIPbS-Ti/TiO$_2$ at + 1 V/Ag|AgCl and 550 W m^{-2} (c) and pH of IF treated solution using IIIPbS-Ti/TiO$_2$ at + 1 V/Ag|AgCl and 550 W m^{-2} (d).

hydroxyl radicals and the highest photocurrent. In contrast, photoelectrodes prepared for four and six SILAR cycles showed lower degradation efficiency than pristine Ti/TiO$_2$. The reduction of PEC efficiency in the case of IVPbS-Ti/TiO$_2$ and VIPbS-Ti/TiO$_2$ photoelectrodes compared to IIPbS-Ti/TiO$_2$ and IIIPbS-Ti/TiO$_2$, despite the greater amount of PbS, was associated with too much PbS nanoparticles and their larger sizes on the Ti/TiO$_2$ surface. This resulted in the formation of agglomerates blocking the TiO$_2$ surface and the flow of photogenerated electrons. Such situation was observed with too many SILAR cycles, which was also reported by Zhu et al. (2015) who investigated number of SILAR cycle on CdS-TiO$_2$ nanocomposites properties. PEC IF degradation in the case of PbS-Ti/TiO$_2$ and pristine Ti/TiO$_2$ occurred according to the pseudo first kinetic order. IF degradation rates constant (Table S3) decreased in order IIIPbS-Ti/TiO$_2$ > IIPbS-Ti/TiO$_2$ > Ti/TiO$_2$ > IVPbS-Ti/TiO$_2$ > VIPbS-Ti/TiO$_2$. The slower PEC degradation, the more electric energy (E$_{EO}$) was consumed for the process.

In Fig. 7b the effect of applied potential on IF PEC degradation

efficiency was presented. The experiments were performed on IIIPbS-Ti/TiO$_2$ at + 0.5 V/Ag=AgCl, + 1 V/Ag=AgCl and + 1.5 V/Ag=AgCl. As can be seen, the most effective degradation was observed at + 1 V/Ag=AgCl. For this process, the IF decomposition rate constant was 0.0148 min^{-1} (Table S3) and was almost twice and 1.5 times higher than k obtained for the process at + 1.5 V/Ag=AgCl and + 0.5 V/Ag=AgCl, respectively. In addition, at + 1 V/Ag=AgCl, more than two times TOC was removed than at other potentials. It was correlated with almost twice lower MCE for + 0.5 V/Ag=AgCl and almost three times for + 1.5 V/Ag=AgCl and in higher electricity consumption. The selection of the appropriate potential depends on the photoanode material and is responsible for the separation of photogenerated charges on the semiconductor and their transport towards the cathode. For the PbS-Ti/TiO$_2$ nanocomposite, the + 1 V/Ag=AgCl was the most advantageous as for pristine Ti/TiO$_2$ (Mazierski et al., 2019). The + 0.5 V/Ag=AgCl turned out to be too low to effectively separate photogenerated charges. In turn, + 1.5 V/Ag=AgCl corresponds to the overpotential of oxygen

release on PbS-Ti/TiO$_2$ and at this potential side reactions such as electrochemical oxidation of water to oxygen can occur.

Photoelectrocatalytic process using IIIPbS-Ti/TiO$_2$ photoelectrode at + 1 V/Ag=AgCl was used to degrade three anticancer drugs, IF, 5-FU and IMB, with different chemical properties and structure. To date, drugs from this group have been removal in such AOPs as photocatalysis (Ofiarska et al., 2016; Fiszka Borzyszkowska et al., 2016) or electrochemical oxidation (Siedlecka et al., 2018), and there was no photoelectrocatalysis applied except our previous research where the pristine Ti/TiO$_2$ photoanode was used (Mazierski et al., 2019). As shown in Fig. 7c and Table S3, all drugs decomposed with similar efficacy and constant rate k as well as comparable E$_{EO}$ consumption. In turn, the highest TOC removal obtained for IF, slightly lower for IMB and the lowest for 5-FU. Additionality, the highest MEC was determined for IMB reaching over 200%, for IF 140% and the lowest for 5-FU of 25.5% (Table S3). In the case of IMB and IF, the MEC value over 100% was the results of generation of photocurrent in the PEC which reduces electric power consumption. The MEC can be over 100% for PEC process because additional photocurrent is generated by the excitation of electrons from the valence band (VB) to conducting band (CB) of the photoanode by irradiation and excited electrons are transport to the cathode. Moreover, the pollutants degradation occurs not only as a result of electrochemical reactions.

In the Fig. 7d the effect of pH of treated IF solution (20 mg L^{-1}) on PEC degradation at + 1 V/Ag=AgCl was presented. As can be seen, PEC degradation efficiency increased with decreasing pH of solution. At acidic pH (pH 3), the highest efficiency of PEC degradation was observed, complete removal of IF occurred after 2 h of the process. On the other hand, at alkaline pH (pH 9), the degradation of IF significantly slowed down and after 3 h of the process only less than 20% of IF was removed. It is worth noting that the pH in the PEC does not affect the surface charge of the photocatalyst (photoanode), which takes place in PC (Garcia-Segura and Brillas, 2017). This is due to the fact that the applied external potential in PEC causes the surface of photoanode positively charged. Hence, more effective degradation at acidic pH is the result of easier mass transport of charges between the solution and the electrodes and higher oxidizing potential of hydroxyl radicals (Mazierski et al., 2019). Moreover, at acidic pH, IF is partially protonated (Mioduszewska et al., 2017), which favors reaction with hydroxyl radicals (Martins et al., 2017). In turn, at the alkaline pH, bicarbonate appear, which are scavengers of radicals and thus the degradation efficiency decrease and IF is in the negative charge form which is more difficult to degrade.

The stability of the IIIPbS-Ti/TiO$_2$ electrode was investigated in five successive cycles (Fig. S3). As shown, the degradation efficiency in the fifth process slightly decreased and was about 90%, which indicates the high stability of the photoelectrode during 900 min of the process. Moreover, concentration of Pb in the treated solution obtained by Atomic Absorption Spectrometry confirmed the release of insignificant amounts of Pb at the level of µg L^{-1}. Furthermore, after the stability test, photoelectrode was re-characterized in terms of DRS UV-Vis, XRD and CA (photocurrent response). Fig. S4 shows obtained results (Supporting Materials). As can be seen when comparing the shape and intensity there are no significant changes in optical, structural or photoelectrochemical properties after stability test which indicates good stability of the obtained photoelectrodes and the possibility of their further use in industrial applications.

3.3. Photoelectrocatalytic mechanism

Photoelectrocatalysis is a process combining photocatalysis with electrochemical oxidation, therefore photoanode material is active in both processes. Nevertheless, the electrochemical oxidation of IF, 5-FU and IMB carried out for IIIPbS-Ti/TiO$_2$ at +1 V did not show any drug degeneration (Fig. S5). It is worth noting that these drugs do not degrade under the direct photolysis (Mazierski et al., 2019; Ofiarska et al., 2016;

Secrétan et al., 2019). In the process of photocatalysis using IIIPbS-Ti/TiO$_2$ (Fig. S5), the decomposition rate constant 5-FU (k = 0.0022 min^{-1}) was almost eight times lower than that obtained in the PEC process (Table S3). A similar trend was also observed for IF and IMB (Fig. S5) where the PEC decomposition rate was higher than PC four and three times, respectively. In addition, only a few percent of TOC removal was observed in the PC, where in the case of PEC it was over 44% for IF, 12.5% for 5-FU and 31% for IMB. Electricity consumption (E$_{EO}$) was even 10 times higher for PC compared to PEC in the case of 5-FU degradation (Table S3). The synergistic effect of photocatalysis and electrochemical oxidation in PEC (Fig. 8) contributes to the reduction of recombination of photogenerated charges (h$^+$/e$^-$) by transporting electrons towards the cathode. It causes, a electrons and holes have a longer lifetime and a greater amount of oxidants can be generated (Mazierski et al., 2019; Daghrir et al., 2012). In the case of photocatalysis using PbS-Ti/TiO$_2$, it is possible to create superoxide radicals by reducing oxygen by photogenerated electrons in the TiO$_2$ conduction band (Zhang et al., 2019a). The photogenerated electrons on PbS conducting band there are not directly involved in reducing O$_2$ to superoxide radicals. What is suggested by generated more superoxide radicals on pristine Ti/TiO$_2$ than PbS-Ti/TiO$_2$ (Fig. 6b). An important part of the mechanism of both PC and PEC is the generation of hydroxyl radicals resulted from water molecules oxidation or OH$^-$ species oxidation by photogenerated h$^+$ in the TiO$_2$. In theory, hydroxyl radicals can also be generated as a result of O$_2^-$ transformation, however, these are rather minor amounts. In addition, pollutions can be degraded by direct oxidation on the photoelectrode surface with h$^+$ participation.

The contribution of individual form of oxidants generated in PEC using PbS-Ti/TiO$_2$ photoelectrode to anticancer drug degradation was determined by reaction with scavengers and was shown in Fig. 9. In the case of IF and 5-FU, degradation of PEC occurred under a similar mechanism. Hydroxyl radicals generated from water or hydroxyl ion oxidation by photogenerated holes had the largest role in the degradation of these drugs (Fig. 9a, b). This is indicated by the greatest inhibition of PEC degradation of IF and 5-FU by MeOH and FA and only slightly weaker process blocking by the single use of scavengers of hydroxyl radicals and h$^+$. The process was inhibited less in the presence of AA than with other scavengers, which indicates a significantly lower contribution of superoxide radicals in PEC drug degradation. It's worth pointing out that superoxide radicals were mainly generated on the cathode in the reaction of oxygen reduction, which indicates a greater amount of radicals generated in the PEC process than in PC (Fig. 6c). On the other hand, in the case of IMB, none of the scavengers (MeOH, AA and FA) decrease efficiency of IMB PEC degradation significantly (Fig. 9c). Hydroxyl and superoxide radicals had a similar but minor impact in the IMB decomposition. These results indicate to participation of other oxidants which can be generated in PEC such as H$_2$O$_2$ or HOO· (Daghrir et al., 2012).

To summarize, the PEC mechanism using PbS-Ti/TiO$_2$ is mainly based on direct and indirect (production OH radicals) activity of photogenerated h$^+$ on valence band of TiO$_2$ and PbS. Superoxide radicals formed as a result of the reduction of oxygen by e$^-$ are less importance in
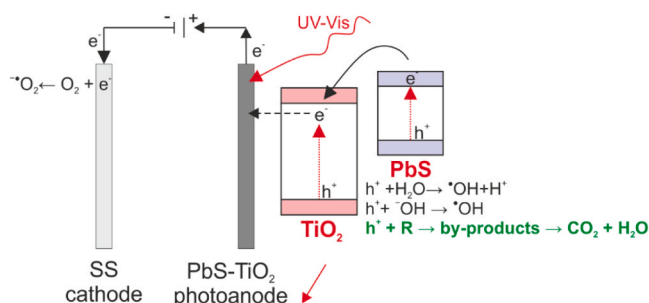

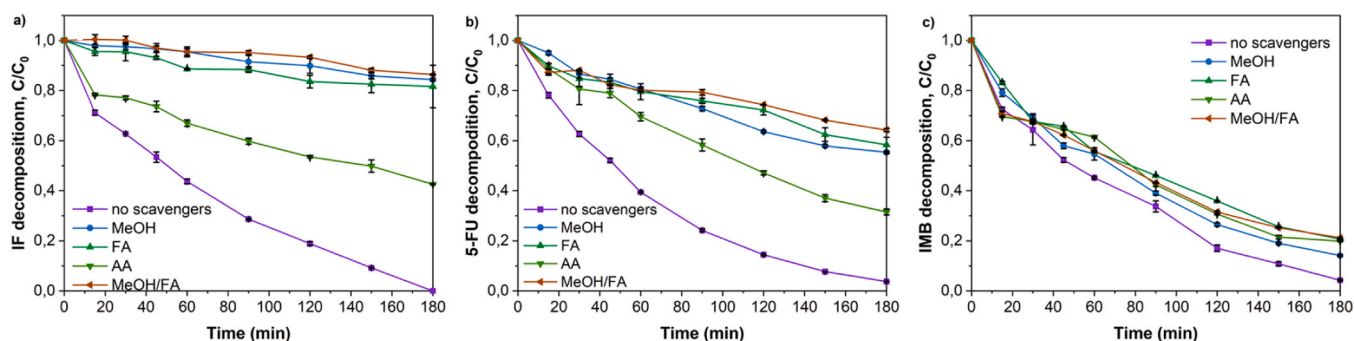**Fig. 8.** General mechanism of photoelectrocatalysis on PbS-TiO$_2$.

Fig. 9. Photoelectrocatalytic degradation using IIIPbS-Ti/TiO$_2$ at + 1 V/ Ag|AgCl and 550 W m^{-2} of IF (20 mg L^{-1}) (a), 5-FU (20 mg L^{-1}) (b) and IMB (20 mg L^{-1}) (c) with scavengers: methanol (MeOH), ascorbic acid (AA) and formic acid (FA).

this process. The main role in the PEC of photogenerated h$^+$ and the hydroxyl radicals generated as a result of h$^+$ activity was observed by other authors (Liu et al., 2018; Yang et al., 2010) and in our previous studies with the use of pristine Ti/TiO$_2$ (Mazierski et al., 2019). However, the presence of PbS nanoparticles on Ti/TiO$_2$ caused an increased direct contribution of h$^+$ in PEC than in the case of pristine Ti/TiO$_2$, which was also observed in the case of decoration of Ti/TiO$_2$ by CdS nanoparticles (Pieczynska et al., 2021). On the other hand, the participation of individual oxidants in the degradation of pollutants depends on the decomposed compound. In the case of IF and 5-FU, hydroxyl radicals were mainly responsible for degradation, while in the case of

IMB another mechanism was dominated.

3.4. Degradation pathway and ecotoxicity

To determine the quality of the obtained solution after photoelectrochemical degradation of anticancer drugs using PbS-Ti/TiO$_2$ photoanode, organic and inorganic degradation products as well as toxicity to duckweed *Lemna minor* were investigated. The proposed degradation pathways for 5-FU, IF and IMB are shown in Fig. 10 and the MS spectra of degradation products were presented in Figs. S6–S8. In the case of 5-FU, two major organic degradation products were identified
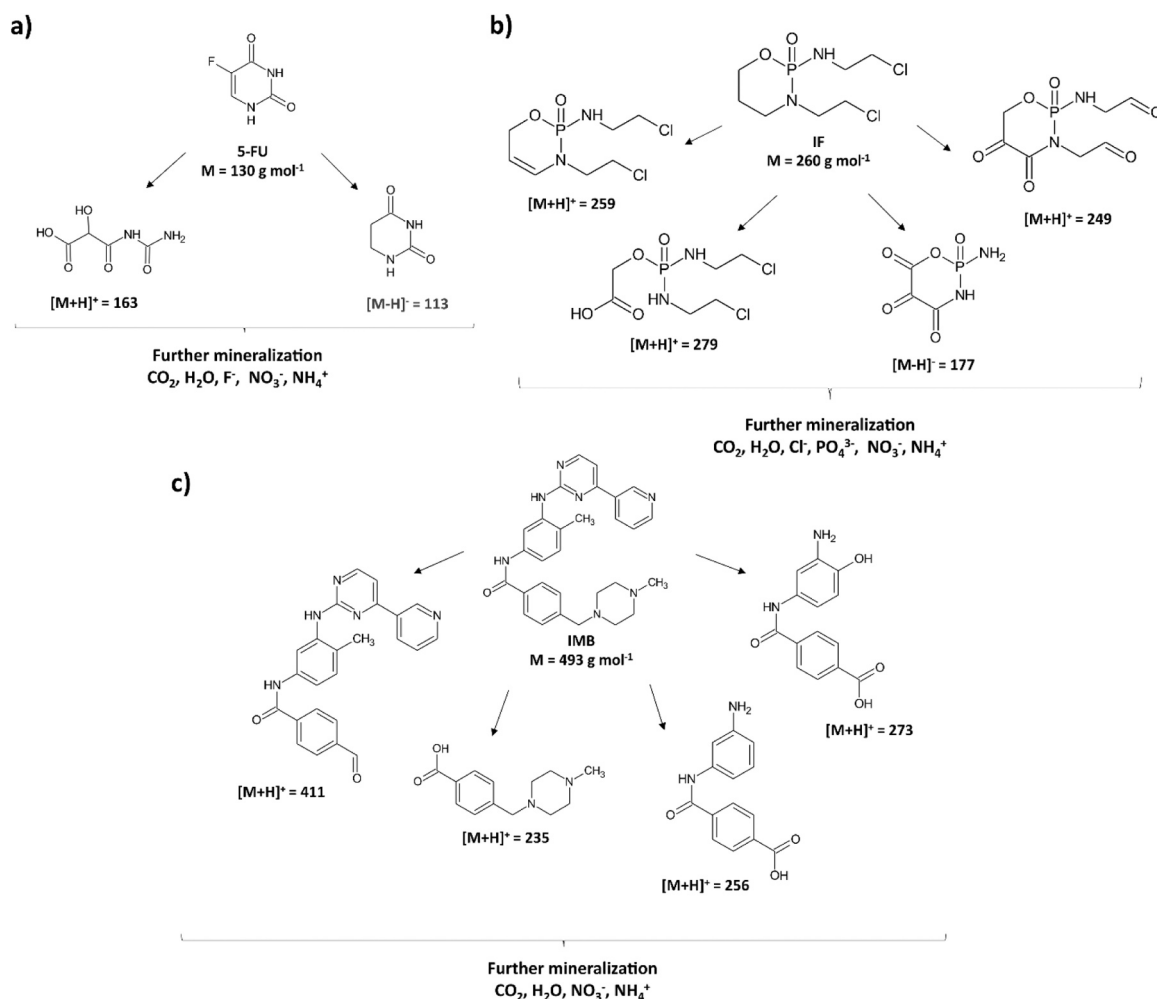

Fig. 10. Photoelectrocatalytic degradation pathway of 5-FU (a), IF (b) and IMB (c) based on identified intermediates by LC-MS.

(Fig. 10a), one with $[M+H]^+ = 163$ which was formed by hydroxylation and breaking of the uracil ring, and the other with $[M-H]^- = 113$ formed by defluorination. Such products have also been identified in the case of PEC degradation of 5-FU using Ti/TiO$_2$ photoelectrode (Mazierski et al., 2019). In a further process stage, the resulting products also decompose into smaller organic compounds and finally mineralization occurs. This is confirmed by the reduction of TOC and the release inorganic ions such fluoride ions in the amount of 27% of the total amount and 14% of nitrogen, mainly in the form of ammonium ions. IF degradation products are shown in Fig. 10b. Compounds with $[M+H]^+ = 249$ and $[M-H]^- = 177$ were formed as a result of kethonization of IF cyclic ring, also dechlorination and detachment of aliphatic chains were observed according to Siedlecka et al. (2018). Imino-ifosfamide ($[M+H]^+ = 259$) was also identified which could have been formed by dehydrogenation as were reported by Česen et al. (2016). The product ($[M+H]^+ = 279$) resulting from ring break was also observed. During the degradation 56% of chloride ions, 32% of nitrogen in the form of nitrate (24%) and ammonium (8%) and 9% of phosphorus in the form of phosphate ions which could be release from IF, were formed. Photoelectrocatalytic degradation of IMB led to the formation of four organic intermediates with $[M+H]^+ = 411$, 273, 256, 235 and release of 30% nitrogen in the form of ammonium (25%) and nitrate (5%) ions (Fig. 10c). Identified degradation products confirm a radical attack on benzyl positions as observed in IMB electrochemical oxidation presented by Siedlecka et al. (2018). As a consequence, C-N bonds broken and some rings detached. In the case of compound with $[M+H]^+ = 411$ the piperazine ring was isolated. When the piperazine, pyridine and pyrimidine rings were removed products with $[M+H]^+ = 273$ and 256 were formed. Compound with $[M+H]^+ = 235$ was generated by pyridine, pyrimidine and phenyl rings detached. Further decomposition led to the formation of increasingly smaller organic compounds such as single rings or short-chain carboxylic acids, followed by mineralization.

Duckweed *Lemna minor* was selected for ecotoxicological studies, which is representative of higher plants potentially exposed to the presence of drug residues in the aquatic environment. In addition, it shows the greatest sensitivity to the presence of these drugs (Białk-Bielińska et al., 2017). It is worth notice that there are few studies on the toxicity of solutions exposed to PEC and that *L. minor* was selected only by us (Mazierski et al., 2019). As shown in Fig. 11, the IF and IMB solution did not inhibit the growth of duckweed both before or after the

photoelectrochemical degradation process. This demonstrates both the lack of toxicity of the drugs and their degradation products. It is worth highlighting the absence of toxicity of the PEC-treated IF solution, because this drug treated by electrochemical oxidation showed increase in growth inhibition of *L.minor* resulted by the generation of toxic chloroorganic degradation products presented in previous studies (Siedlecka et al., 2018). In the case of 5-FU, the initial solution showed 65% growth inhibition of *L.minor*. With the photoelectrocatalytic degradation and decreasing drug concentration, a decrease in toxicity was observed (Fig. 11). This indicates that the formed degradation products are less toxic than the parent compound. A decrease in *L.minor* growth inhibition in PEC degradation of 5-FU was also observed when a Ti/TiO$_2$ photoelectrode were used (Mazierski et al., 2019). In summary, the obtained solutions after photoelectrochemical degradation of IF, 5-FU and IMB, despite incomplete mineralization, did not show toxicity to a representative of higher plants, which leads to the claim that the use of PbS-Ti/TiO$_2$ in PEC is a safe and promising method for drug treatment.

4. Conclusion

Sensitization of TiO$_2$ photoelectrodes by PbS QDs increased the efficiency of PEC degradation of anticancer drugs and it depends on the amount and size of PbS nanoparticles. The more SILAR cycles, the greater amount and the larger size of PbS QDs on the TiO$_2$ surface, as well the absorption of irradiation in the range of visible light also increases. However, the highest efficiency of drug degradation was achieved with the use of the electrode padded at 3 SILAR cycles, which mainly contained PbS QDs with dimensions from 2 nm to 4 nm. This photoelectrode also showed the highest photocurrent generation. In the case of more SILAR cycles (4 and 6) applying for electrode preparation, agglomeration of PbS QDs on the Ti/TiO$_2$ surface and a decrease in PEC activity was observed. Improving the PEC efficiency of the PbS-Ti/TiO$_2$ electrode in relation to pristine Ti/TiO$_2$ resulted from several aspects: (i) enhanced the absorption of irradiation in the visible light range; (ii) generating additional h$^+$ in the VB of PbS involve in degradation of pollutants and (iii) reducing recombination of e$^-$/h$^+$ pairs. It's worth pointing out, although the rates of PEC degradation of 5-FU, IF and IMB were similar, the contribution of individual oxidants in the drugs degradation were different, which may indicate a different mechanism of PEC degradation depending on the chemical structure of the drug. In the case of 5-FU, there was a decrease in toxicity to *L. minor* with decreasing drug concentration, while in the case of IF and IMB, no toxicity was observed throughout the PEC process.

CRediT authorship contribution statement

Paweł Mazierski: Investigation, Writing – original draft, Project administration. **Patrycja Wilczewska**: Investigation. **Wojciech Lisowski**: Investigation. **Tomasz Klimczuk**: Investigation. **Anna Białk-Bielińska**: Investigation. **Adriana Zaleska-Medynska**: Visualization, Writing – review & editing. **Ewa Siedlecka**: Writing – review & editing. **Aleksandra Pieczyńska**: Supervision, Investigation, Writing – original draft, Funding acquisition, Project administration, Writing – review & editing.

Declaration of Competing Interest

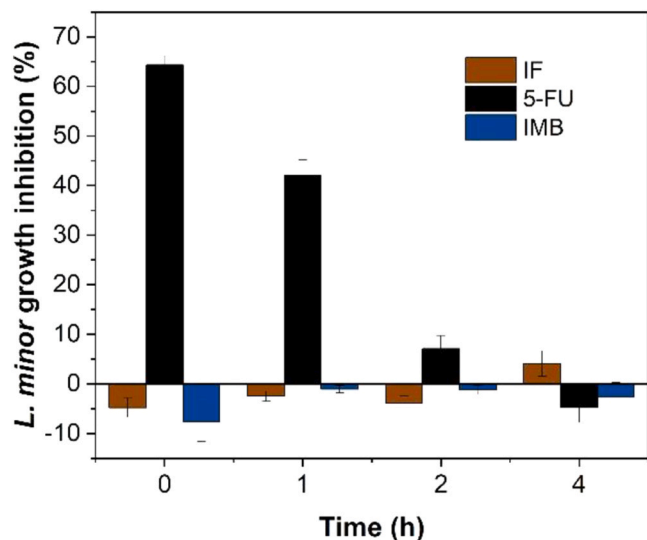The authors declare that they have no known competing financial

Fig. 11. Normalized response of IF (50 mg L^{-1}), 5-FU (50 mg L^{-1}) and IMB (50 mg L^{-1}) during PEC degradation using IIIPbS-Ti/TiO$_2$ at $+ 1$ V/ AglAgCl and 550 W m^{-2} for the *Lemna minor* growth inhibition.

interests or personal relationships that could have appeared to influence the work reported in this paper.

Acknowledgments

Authors would like thank Łukasz Grabarczyk for the ecotoxicity tests and the National Science Center (Poland) for financial support under the grant no 2015/19/D/ST5/00710.

Appendix A. Supporting information

Supplementary data associated with this article can be found in the online version at doi:10.1016/j.jhazmat.2021.126751.

References

Białk-Bielińska, A., Mulkiewicz, E., Stokowski, M., Stolte, S., Stepnowski, P., 2017. Acute aquatic toxicity assessment of six anti-cancer drugs and one metabolite using biotest battery – biological effects and stability under test conditions. Chemosphere 189, 689–698. https://doi.org/10.1016/j.chemosphere.2017.08.174.

Česen, M., Kosjek, T., Busetti, F., Kompare, B., Heath, E., 2016. Human metabolites and transformation products of cyclophosphamide and ifosfamide: analysis, occurrence and formation during abiotic treatments. Environ. Sci. Pollut. Res. 23, 11209–11223. https://doi.org/10.1007/s11356-016-6321-1.

Chatzitakis, A., Papaderakis, Karanasios, N., Georgieva, J., Pavlidou, E., Litsardakis, G., Poulios, I., Sotiropoulos, S., 2017. Comparison of the photoelectrochemical performance of particulate and nanotube TiO2 photoanodes. Catal. Today 280, 14–20. https://doi.org/10.1016/j.cattod.2016.07.017.

Cheng, X., Liu, H., Chen, Q., Li, J., Wang, P., 2013. Preparation and characterization of palladium nano-crystallite decorated TiO 2 nano-tubes photoelectrode and its enhanced photocatalytic efficiency for degradation of diclofenac. J. Hazard. Mater. 254–255, 141–148. https://doi.org/10.1016/j.jhazmat.2013.03.062.

Collivignarelli, M.C., Abbà, A., Carnevale Miino, M., Bertanza, G., Sorlini, S., Damiani, S., Arab, H., Bestetti, M., Franz, S., 2021. Photoelectrocatalysis on TiO2 meshes: different applications in the integrated urban water management. Environ. Sci. Pollut. Res. https://doi.org/10.1007/s11356-021-12606-5.

Daghrir, R., Drogui, P., Robert, D., 2012. Photoelectrocatalytic technologies for environmental applications. J. Photochem. Photobiol. A Chem. 238, 41–52. https://doi.org/10.1016/j.jphotochem.2012.04.009.

Daghrir, R., Drogui, P., Delegan, N., El Khakani, M.A., 2014. Removal of chlortetracycline from spiked municipal wastewater using a photoelectrocatalytic process operated under sunlight irradiations. Sci. Total Environ. 466–467, 300–305. https://doi.org/10.1016/j.scitotenv.2013.07.001.

Deng, X., Zhang, H., Guo, R., Cui, Y., Ma, Q., Zhang, X., 2018a. Effect of fabricating parameters on photoelectrocatalytic performance of CeO2/TiO2 nanotube arrays photoelectrode. Sep. Purif. Technol. 193, 264–273. https://doi.org/10.1016/j.seppur.2017.10.066.

Deng, X., Zhang, H., Guo, R., Ma, Q., Cui, Y., Cheng, X., Xie, M., Cheng, Q., 2018b. Effect of Ti 3+ on enhancing photocatalytic and photoelectrochemical properties of TiO 2 nanorods/nanosheets photoelectrode. Sep. Purif. Technol. 192, 329–3339.

Fiszka Borzyszkowska, A., Pieczyńska, A., Ofiarska, A., Nikiforow, K., Stepnowski, P., Siedlecka, E.M., 2016. Bi-B-TiO2-based photocatalytic decomposition of cytostatic drugs under simulated sunlight treatments. Sep. Purif. Technol. 169, 113–120. https://doi.org/10.1016/j.seppur.2016.06.012.

Garcia-Segura, S., Brillas, E., 2017. Applied photoelectrocatalysis on the degradation of organic pollutants in wastewaters. J. Photochem. Photobiol. C Photochem. Rev. 31, 1–35. https://doi.org/10.1016/j.jphotochemrev.2017.01.005.

Guo, H., Li, L., Su, C., Yu, D., Liu, Z., 2021. Effective photocathodic protection for 304 stainless steel by PbS quantum dots modified TiO2 nanotubes. Mater. Chem. Phys. 258, 123914 https://doi.org/10.1016/j.matchemphys.2020.123914.

Hajjaji, A., Jemai, S., Rebhi, A., Trabelsi, K., Gaidi, M., Alhazaa, A.N., Al-Gawati, M.A., El Khakani, M.A., Bessais, B., 2020. Enhancement of photocatalytic and photoelectrochemical properties of TiO2 nanotubes sensitized by SILAR - deposited PbS nanoparticles. J. Mater. 6, 62–69. https://doi.org/10.1016/j.jmat.2019.12.002.

Huang, B., Yang, W., Wen, Y., Shan, B., Chen, R., 2015. Co3O4-Modified TiO2 Nanotube Arrays via Atomic Layer Deposition for Improved Visible-Light Photoelectrochemical Performance. ACS Appl. Mater. Interfaces 7 (1), 422–431.

Isidori, M., Lavorgna, M., Russo, C., Kundi, M., Knasmueller, S., Miren, L., Kosjek, T., Heath, E., Cesen, M., Janez, S., 2016. Chemical and toxicological characterisation of anticancer drugs in hospital and municipal wastewaters from Slovenia and Spain. Environ. Pollut. 219, 275–287. https://doi.org/10.1016/j.envpol.2016.10.039.

Jia, M., Hu, X., Wang, S., Huang, Y., Song, L., 2015. Photocatalytic properties of hierarchical BiOXs obtained via an ethanol-assisted solvothermal process. J. Environ. Sci. 35, 172–180. https://doi.org/10.1016/j.jes.2014.09.045.

Liu, D., Tian, R., Wang, J., Nie, E., Piao, X., Li, X., Sun, Z., 2017. Photoelectrocatalytic degradation of methylene blue using F doped TiO2 photoelectrode under visible light irradiation. Chemosphere 185, 574–581. https://doi.org/10.1016/j.chemosphere.2017.07.071.

Liu, D., Zhou, J., Wang, J., Tian, R., Li, X., Nie, E., Piao, X., Sun, Z., 2018. Enhanced visible light photoelectrocatalytic degradation of organic contaminants by F and Sn co-doped TiO2 photoelectrode. Chem. Eng. J. 344, 332–341. https://doi.org/10.1016/j.cej.2018.03.103.

Liu, Z., Wang, B., Wu, J., Dong, Q., Zhang, X., Xu, H., 2016. Effects of hydroxylation on PbS quantum dot sensitized TiO2 nanotube array photoelectrodes. Electrochim. Acta 187, 480–487. https://doi.org/10.1016/j.electacta.2015.11.042.

Ma, Q., Wang, H., Zhang, H., Cheng, X., Xie, M., 2017. Fabrication of MnO2/TiO2 nanotube arrays photoelectrode and its enhanced visible light photoelectrocatalytic performance and mechanism. Sep. Purif. Technol. 189, 193–203. https://doi.org/10.1016/j.seppur.2017.08.007.

Ma, Q., Zhang, H., Cui, Y., Deng, X., Guo, R., Cheng, X., Xie, M., Cheng, Q., 2018. Fabrication of Cu2O/TiO2 nano-tube arrays photoelectrode and its enhanced photoelectrocatalytic performance for degradation of 2, 4, 6- trichlorophenol. J. Ind. Eng. Chem. 57, 181–187. https://doi.org/10.1016/j.jiec.2017.08.020.

Martins, A.S., Nuñez, L., Roberto, M., Lanza, D.V., 2017. Enhanced photoelectrocatalytic performance of TiO 2 nanotube array modi fi ed with WO 3 applied to the degradation of the endocrine disruptor propyl paraben. J. Electroanal. Chem. 802, 33–39. https://doi.org/10.1016/j.jelechem.2017.08.040.

Mazierski, P., Nadolna, J., Nowaczyk, G., Lisowski, W., Winiarski, J., Klimczuk, T., Piotr, M., Jurga, S., Zaleska-medynska, A., 2017. Highly visible-light-photoactive heterojunction based on TiO2 nanotubes decorated by Pt nanoparticles and Bi2S3 quantum dots. J. Phys. Chem. C. https://doi.org/10.1021/acs.jpcc.7b03895.

Mazierski, P., Fiszka Borzyszkowska, A., Wilczewska, P., Białk-Bielinska, A., Zaleska-Medynska, A., Siedlecka, E.M., Pieczy?nska, A., 2019. Removal of 5- fluorouracil by solar-driven photoelectrocatalytic oxidation using Ti/TiO2 (NT) photoelectrodes. Water Res. 157, 610–620. https://doi.org/10.1016/j.watres.2019.04.010.

Mioduszewska, K., Dołżonek, J., Wyrzykowski, D., Kubik, Ł., Wiczling, P., Sikorska, C., Toński, M., Kaczyński, Z., Stepnowski, P., Białk-Bielińska, A., 2017. Overview of experimental and computational methods for the determination of the pKa values of 5-fluorouracil, cyclophosphamide, ifosfamide, imatinib and methotrexate. TrAC Trends Anal. Chem. 97, 283–296. https://doi.org/10.1016/j.trac.2017.09.009.

Mohite, V.S., Mahadik, M.A., Kumbhar, S.S., Kothavale, V.P., Moholkar, A.V., Rajpure, K. Y., Bhosale, C.H., 2015. Photoelectrocatalytic degradation of benzoic acid using sprayed TiO 2 thin fi lms. Ceram. Int. 41, 2202–2208. https://doi.org/10.1016/j.ceramint.2014.10.020.

Naumkin, A.V., Kraut-Vass, A., Gaarenstroom, S.W., Powell, C.J., 2010. NIST X-ray Photoelectron Spectroscopy Database, NIST Stand. Ref. Database. 20.

Ofiarska, A., Pieczyńska, A., Fiszka Borzyszkowska, A., Stepnowski, P., Siedlecka, E.M., 2016. Pt–TiO2-assisted photocatalytic degradation of the cytostatic drugs ifosfamide and cyclophosphamide under artificial sunlight. Chem. Eng. J. 285, 417–427. https://doi.org/10.1016/j.cej.2015.09.109.

Olvera-Rodríguez, I., Hernández, R., Medel, A., Guzmán, C., 2019. TiO2/Au/TiO2 multilayer thin-film photoanodes synthesized by pulsed laser deposition for photoelectrochemical degradation of organic pollutants. Sep. Purif. Technol. 224, 189–198. https://doi.org/10.1016/j.seppur.2019.05.020.

Pieczynska, A., Mazierski, P., Lisowski, W., Klimczuk, T., Zaleska-Medynska, A., Siedlecka, E., 2021. Effect of synthesis method parameters on properties and photoelectrocatalytic activity under solar irradiation of TiO2nanotubes decorated with CdS quantum dots. J. Environ. Chem. Eng. 9, 104816 https://doi.org/10.1016/j.jece.2020.104816.

Pieczyńska, A., Borzyszkowska, A.F., Siedlecka, E.M., 2017. Removal of cytostatic drugs by AOPs: a review of applied processes in the context of green technology. Crit. Rev. Environ. Sci. Technol. 47, 1282–1335. https://doi.org/10.1080/10643389.2017.1370990.

Rahna, N.B., Kalarivalappil, V., Nageri, M., Pillai, S.C., Hinder, S.J., Kumar, V., Vijayan, B.K., 2016. Stability studies of PbS sensitised TiO 2 nanotube arrays for visible light photocatalytic applications by X-ray photoelectron spectroscopy (XPS). Mater. Sci. Semicond. Process. 42, 303–310. https://doi.org/10.1016/j.mssp.2015.10.025.

Reiche, R., Thielsch, R., Oswald, S., Wetzig, K., 1999. XPS studies and factor analysis of PbS nanocrystal-doped SiO2 thin films. J. Electron Spectrosc. Relat. Phenom. 104, 161–171. https://doi.org/10.1016/s0368-2048(98)00326-0.

Santos, S.F., Franquet-griell, H., Lacorte, S., Madeira, L.M., 2017. Anticancer drugs in Portuguese surface waters e Estimation of concentrations and identification of potentially priority drugs. Chemosphere 184, 1250–1260. https://doi.org/10.1016/j.chemosphere.2017.06.102.

Secrétan, P.H., Karoui, M., Sadou-Yaye, H., Levi, Y., Tortolano, L., Solgadi, A., Yagoubi, N., Do, B., 2019. Imatinib: major photocatalytic degradation pathways in aqueous media and the relative toxicity of its transformation products. Sci. Total Environ. 655, 547–556. https://doi.org/10.1016/j.scitotenv.2018.11.270.

Siedlecka, M.E., Ofiarska, A., Fiszka Borzyszkowska, A., Białk-Bielińska, A., Stepnowski, P., Pieczyńska, A., 2018. Cytostatic drug removal using electrochemical oxidation with BDD electrode: degradation pathway and toxicity. Water Res. 144, 235–245. https://doi.org/10.1016/j.watres.2018.07.035.

Su, Y., Wang, G., Ta, D., Kuo, F., Chang, M., Shih, Y., 2016. Photoelectrocatalytic degradation of the antibiotic sulfamethoxazole using TiO2/Ti photoanode. Appl. Catal. B Environ. 186, 184–192. https://doi.org/10.1016/j.apcatb.2016.01.003.

Wu, J., Xu, H., Yan, W., 2016. Photoelectrocatalytic degradation Rhodamine B over highly ordered TiO2 nanotube arrays photoelectrode. Appl. Surf. Sci. 386, 1–13. https://doi.org/10.1016/j.apsusc.2016.05.155.

Xin, Y., Liu, H., Han, L., Zhou, Y., 2011. Comparative study of photocatalytic and photoelectrocatalytic properties of alachlor using different morphology TiO2/Ti photoelectrodes. J. Hazard. Mater. 192, 1812–1818, 1812–1812.

Xu, Y., Zhang, M., Lv, J., Zhang, M., Jiang, X., 2014. Preparation and characterization of heat-assisted PbS/TiO 2 thin films. Appl. Surf. Sci. 317, 1035–1040. https://doi.org/10.1016/j.apsusc.2014.08.173.

Yang, J., Dai, J., Chen, C., Zhao, J., 2010. Effects of hydroxyl radicals and oxygen species on the 4-chlorophenol degradation by photoelectrocatalytic reactions with TiO2-film electrodes. J. Photochem. Photobiol. A Chem. 208, 66–77. https://doi.org/10.1016/j.jphotochem.2009.08.007.

Ye, Y., Bruning, H., Li, X., Yntema, D., Rijnaarts, H.H.M., 2018. Significant enhancement of micropollutant photocatalytic degradation using a TiO 2 nanotube array photoanode based photocatalytic fuel cell. Chem. Eng. J. 354, 553–562. https://doi.org/10.1016/j.cej.2018.08.064.

Yu, L., Wang, D., Ye, D., 2015. CdS nanoparticles decorated anatase TiO 2 nanotubes with enhanced visible light photocatalytic activity. Sep. Purif. Technol. 156, 708–714. https://doi.org/10.1016/j.seppur.2015.10.069.

Zhang, H., Gao, Y., Zhu, G., Li, B., Gou, J., Cheng, X., 2019. Synthesis of PbS/TiO2 nano-tubes photoelectrode and its enhanced visible light driven photocatalytic performance and mechanism for purification of 4-chlorobenzoic acid. Sep. Purif. Technol. 227, 115697 https://doi.org/10.1016/j.seppur.2019.115697.

Zhang, X., Wang, B., Liu, Z., 2016. Tuning PbS QDs deposited onto TiO 2 nanotube arrays to improve photoelectrochemical performances. J. Colloid Interface Sci. 484, 213–219. https://doi.org/10.1016/j.jcis.2016.09.002.

Zhang, X., Gao, Y., chao Nengzi, L., Li, B., Gou, J., Cheng, X., 2019. Synthesis of SnS/TiO2 nano-tube arrays photoelectrode and its high photoelectrocatalytic

performance for elimination of 2,4,6-trichlorophenol. Sep. Purif. Technol. 228, 115742 https://doi.org/10.1016/j.seppur.2019.115742.

Zhang, Y., Xiong, X., Han, Y., Zhang, X., Shen, F., Deng, S., Xiao, H., Yang, X., Yang, G., Peng, H., 2012. Photoelectrocatalytic degradation of recalcitrant organic pollutants using TiO2 film electrodes: an overview. Chemosphere 88, 145–154. https://doi.org/10.1016/j.chemosphere.2012.03.020.

Zhou, C., Geng, Y., Chen, Q., Xu, J., Huang, N., Gan, Y., Zhou, L., 2016. A novel PbS/TiO2 composite counter electrode for CdS quantum dot-sensitized ZnO nanorods solar cells. Mater. Lett. 172, 171–174. https://doi.org/10.1016/j.matlet.2016.02.092.

Zhou, R., Xu, J., Huang, F., Ji, F., Wan, L., Niu, H., Mao, X., Xu, J., Cao, G., 2016. A novel anion-exchange strategy for constructing high performance PbS quantum dot-sensitized solar cells. Nano Energy 30, 559–569. https://doi.org/10.1016/j.nanoen.2016.10.052.

Zhou, X., Zheng, Y., Zhou, J., Zhou, S., 2015. Degradation kinetics of photoelectrocatalysis on landfill leachate using codoped TiO2/Ti photoelectrodes. J. Nanomater. 2015, 1–11. https://doi.org/10.1155/2015/810579.

Zhu, Y., Wang, Y., Chen, Z., Qin, L., Yang, L., Zhu, L., Tang, P., Gao, T., Huang, Y., Sha, Z., Tang, G., 2015. Visible light induced photocatalysis on CdS quantum dots decorated TiO2 nanotube arrays. Appl. Catal. A Gen. 498, 159–166. https://doi.org/10.1016/j.apcata.2015.03.035.